# Emitting Excitonic Polaron States in Core LH1 and Peripheral LH2 Bacterial Light-Harvesting Complexes†

**Kõu Timpmann,‡ Margus Rätsep,‡ C. Neil Hunter,§ and Arvi Freiberg*,‡,#**

*Institute of Physics, University of Tartu, Riia 142, Tartu 51014, Estonia, Institute of Molecular and Cell Biology, University of Tartu, Riia 23, Tartu 51010, Estonia, and Krebs Institute of Biomolecular Research, University of Sheffield, Firth Court Western Bank, Sheffield, S10 2TN, United Kingdom*

*Received: February 24, 2004*

Hole-burned absorption and line-narrowed fluorescence spectra along with nanosecond fluorescence decay kinetics have been studied at 5 K in core LH1 and peripheral LH2 antenna complexes isolated from the photosynthetic purple bacterium *Rhodobacter sphaeroides*. A dual nature for the respective emission bands has been confirmed in both complexes and has been assigned to the nearly free excitons weakly coupled to lattice vibrations and to the strongly coupled self-trapped excitons. The apparent phonon structure of quasi-free excitons has been analyzed resulting in a total Huang−Rhys factor, a characteristic of the electron−phonon coupling strength, equal to $S = 0.85 \pm 0.10$ in LH1 and to $S = 1.05 \pm 0.10$ in LH2. An estimate for self-trapped excitons is a few times larger. Excitonic polarons are thus proper excitations in LH1 and LH2 complexes, as the electron−phonon coupling cannot be ignored.

## 1. Introduction

Excitons (more generally, excitons coupled to lattice vibrations or excitonic polarons) are common light excitations in pigment aggregates of photosynthetic antenna complexes (see ref 1 for a review). Yet, in most cases, knowledge about the exciton level structure and its characteristic parameters is far from complete. Here, we concentrate on the lowest energy exciton states of bacteriochlorophyll *a*-containing light-harvesting (LH) pigment−protein complexes, which determine the utilization of solar energy in photosynthetic bacteria. In purple bacteria two types of LH complexes, named the core (LH1) and the peripheral (LH2) complexes, can be found. The crystal structure of these complexes is known with nearly atomic precision.[2,3] The photoactive part of the complexes we are concerned with here consists of 30−32 (LH1) or 18 (LH2) bacteriochlorophyll *a* (Bchl) molecules in a circular quasi-one-dimensional arrangement.

A weak spectral structure has been resolved and characterized at the long-wavelength slope of the lowest absorption band, related to the $Q_y$ absorption of Bchl molecules, of both complexes by zero-phonon hole (ZPH) action spectroscopy.[4] The ZPH action spectrum for LH2 (commonly referred to as B870) from *Rhodobacter (Rb.) sphaeroides*, for example, lies 185−204 $cm^{-1}$ below the maximum of the main (B850) absorption band and carries only a few percent of its integrated intensity.[4,5] Some variation of experimental parameters has been observed, depending on the sample origin and quality.[4−8] A common interpretation based on the weakly disordered exciton model[4] is that the B870 sub-band represents an inhomogeneous distribution of the lowest energy $\mathbf{k} = 0$ exciton states of LH2.

A phonon structure of the spectra related to the B870 sub-band has recently been analyzed using simultaneously two spectrally selective techniques—hole burning (HB) and fluorescence line narrowing (FLN).[8] As a result, a genuine single-exciton state absorption/emission profile was established. The profile consists of a narrow zero-phonon line (ZPL) and a broad but structured phonon sideband (PSB) characterized by a total Huang−Rhys factor of $S = 0.8 \pm 0.2$. The Huang−Rhys factor is a measure of a linear electron coupling strength and determines the mean number of vibrational quanta accompanying an electronic transition. We notice that the number established in ref 8 is larger than that previously estimated based solely on HB measurements.[4]

Provided the B870 sub-band represents the inhomogeneous distribution of the $\mathbf{k} = 0$ exciton states of LH2, one expects at low temperatures only resonant fluorescence with the phonon sideband established in ref 8 to be observed upon excitation within this band. Similarly at nonresonant/broadband excitation, as a result of B870 being the lowest exciton state and from the limited Huang−Rhys factor obtained, one expects a fluorescence spectrum with only a small red shift (i.e., a shift toward longer wavelengths) relative to the B870 peak. Direct numerical convolution of the established single-exciton state emission profile with the B870 band shape yields a red shift of ∼29 $cm^{-1}$.[9] This is in obvious disagreement with the experiment, as noticed in refs 7 and 10. The observed LH2 emission spectrum is broad and considerably more red-shifted in comparison with the B870 band under both resonant and nonresonant excitation (Figure 1). Spectrally selective excitation within the B870 band results only in minor narrowing of the fluorescence band, suggesting that there must be at least two overlapping fluorescence components (the one characterized with $S = 0.8 \pm 0.2$ and the second one, with considerably larger electron−phonon coupling strength). To account for these latter observations, it was proposed in ref 10 that the strongly coupled emitting states belong to the dynamically self-trapped excitons. This idea was advanced both experimentally and theoretically in ref 7. A characteristic spectroscopic effect of the self-trapping is a structureless homogeneously broadened emission band signifi-

† Part of the special issue "Gerald Small Festschrift".

* Corresponding author: Fax: +3727-383033. E-mail: freiberg@fi.tartu.ee.
‡ Institute of Physics, University of Tartu.
# Institute of Molecular and Cell Biology, University of Tartu.
§ University of Sheffield.

10.1021/jp049165a CCC: $27.50 
Published on Web 05/06/2004

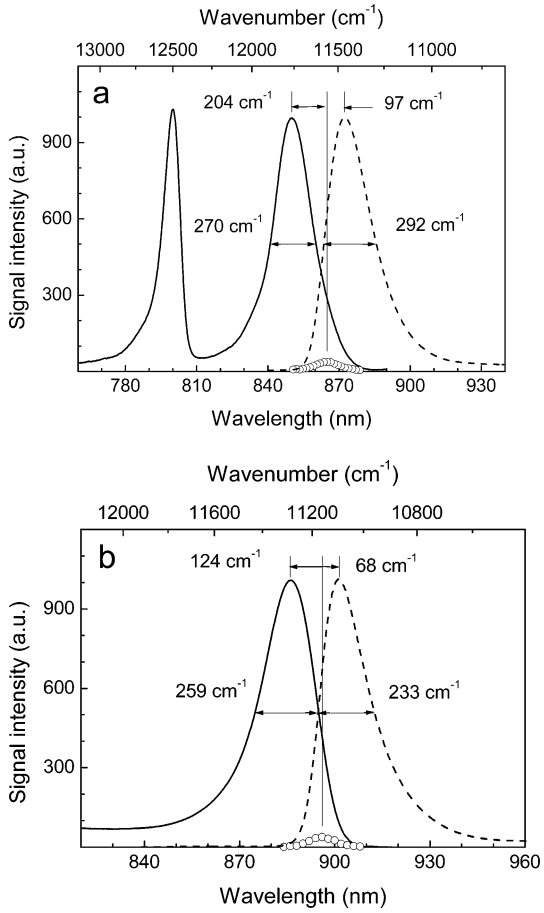


**Figure 1.** Peak-normalized absorption (solid curves) and nonselectively excited fluorescence (dashed curve) spectra for purified LH2 (a) and LH1 (b) complexes from *Rb. sphaeroides* at 5 K. Shown at the red tail of the absorption spectra are the zero-phonon hole action spectra obtained with 1.2 J/cm$^2$ constant fluence for LH2 and with 0.03 J/cm$^2$ for LH1. The action spectra are magnified ∼8 and ∼5 times, respectively, relative to the absorbance scale for better visibility.

cantly red-shifted relative to the absorption band. Quantitative aspects of the phenomenon, such as the precise shape of the self-trapped exciton emission spectrum, however, remained obscure.

In this work, apart from further elaborating the data on LH2 by studying excitation saturation effects, we extend our investigations to LH1 antenna complexes. Some measurements have also been performed on membranes prepared from an LH1-only mutant,[11] which contain a network of electronically coupled core antenna complexes. Special attention has been paid to the possible heterogeneous nature of exciton emission spectra and to characterization of the component spectra in terms of shape and electron−phonon coupling strength. Compared with our previous study,[8] considerable effort has been taken to minimize scattered laser light. The improved technology ensured almost undisturbed recording of the resonance fluorescence spectrum (including both its ZPL and phonon sideband parts) for the first time in the differential FLN experimental scheme.

## 2. Materials and Methods

**Sample Preparation.** The LH1 and LH2 complexes from *Rb. sphaeroides* were prepared as described in refs 12 and 13 respectively. The samples were diluted in a mixture of a buffer (15 mM Tris, pH 8.0) and glycerol (1:2 volume ratio) to yield a desired absorbance in the sample cell and to obtain good optical quality glass at low-temperature measurements. To maintain the LH1 and LH2 complexes as well-separate units over long period of experimental time, specific detergent was added to the final sample solution: DHPC (3 mM) in case of LH1 complexes and LDAO (∼1%) in case of LH2 complexes. During measurements the samples were contained in acrylic cuvettes of 10 mm optical path length with an optical density of 0.6−0.9 at the maximum of the absorption spectrum (resulting in an optical density of <0.15 at the actual wavelengths of measurements), which is sufficiently low to avoid systematic errors due to reabsorption.

**Experimental Methodology.** A continuous-wave Ti:Sapphire solid state laser (Model 3900S, Spectra Physics) with line width of 0.5 cm$^{-1}$ was used for HB and FLN experiments. For transmission measurements, a 12 V tungsten lamp was employed. Detection was performed with a spectral resolution of 0.1 nm using a 0.6 m spectrograph (MDR-23, LOMO, Russia) combined with an electrically cooled CCD camera (Andor Technology, UK). The sample temperature, 5 K, was maintained using a helium bath cryostat (Utreks, Ukraine) and a temperature controller with the calibrated Si diode. The experimental setup allowed the study of the absorption and fluorescence spectra from the same sample volume in consecutive steps. First the absorption spectrum was measured by using the white probe beam from the tungsten lamp. The spatial profile of the beam was properly modified with pinholes and attenuated by color and neutral filters. Second, the FLN spectrum was measured at an excitation wavelength using the lowest possible excitation level to avoid unwanted HB processes at this stage. A typical FLN spectrum, for example, in LH2 was recorded in 40 s using the excitation intensity of 1 mW/cm$^2$. Only minor changes in fluorescence yield were observed during two successive measurements under those conditions. Also the absorption spectrum remained almost unchanged (fractional absorbance change less than 0.5%) indicating that the HB effects during the FLN measurements appear to be negligible at the applied excitation fluence of 0.04 J/cm$^2$. The subsequent experimental steps include the intentional modification of the sample absorption (hole burning) by irradiation of the sample with the laser at burn wavelength followed by postburn absorption and FLN measurements. The difference between the preburn and postburn absorption spectra yields the persistent HB spectrum, and that between the emission spectra, the difference fluorescence line-narrowing (ΔFLN) spectrum corresponding to the HB spectrum. We stress that the ΔFLN spectrum shows the contribution of the signal that has been lost due to hole burning, that is, it corresponds to the sites/states that were burnt out during irradiation. Since the methodology used employs both FLN and HB measurements, it can be regarded as a kind of double spectral selection technique. A similar technique has been developed and applied for impurity molecules in solids.[14,15] It was recently revived in our laboratory in the context of delocalized exciton spectra.[8]

Compared with our previous study,[8] considerable effort was taken to minimize scattered laser light. This was achieved by controlling the quality of the glassy sample, by special design of the cuvette holder, by careful selection of optics, and by spatial filtering of the excitation laser beam. The combined measures ensured sufficiently low-level scattering, comparable or even lower than the ZPL intensity of the sample fluorescence, and allowed almost undisturbed recording of the resonance fluorescence spectrum (including both its ZPL and phonon side band components) in the differential FLN experimental scheme.

Fluorescence lifetimes were measured using a picosecond spectrochronograph setup based on a Synchroscan streak camera

and described in detail earlier.[16] The typical width of the temporal response function during these measurements was ~30 ps.

**Data Analysis.** The measured FLN spectra have been analyzed using the localized exciton model introduced by Hayes et al.[17] and applied to FLN by Pieper et al.[18,19] The following paragraphs give a brief summary of the expressions used in our calculations.

For linear Franck−Condon coupling to a distribution of harmonic phonons the single site/state absorption and fluorescence profiles in the low-temperature limit are given as[17]

$$F(\omega) = \mathrm{e}^{-S}\, l_0(\omega - \Omega) + \sum_{R=1}^{\infty} S^R \frac{\mathrm{e}^{-S}}{R!}\, l_R(\omega - \Omega \mp R\omega_\mathrm{m}) \quad (1)$$

Here, the $-R\omega_\mathrm{m}$ and $+R\omega_\mathrm{m}$ terms correspond to absorption and fluorescence, respectively, $l_0(\omega - \Omega)$ is the ZPL shape with the maximum at frequency $\Omega$. The apparent phonon sideband of the ZPL consists of all $R$-phonon transitions ($R \geq 1$) with normalized line shapes $l_R(\omega - \Omega \mp R\omega_\mathrm{m})$ peaking at $\Omega \mp R\omega_\mathrm{m}$ ($\omega_\mathrm{m}$ is the mean phonon frequency). The relative contribution of the component spectra is determined by a Poisson type weighting factor for every $R$ with the Huang−Rhys factor $S$. The one-phonon profile $l_1(\omega - \Omega \mp \omega_\mathrm{m})$ provides essential information about the density of states of phonon modes in the system and about their coupling to the electronic degrees of freedom. It also uniquely determines the shape of all $l_R$ profiles with $R>1$.

The nonselectively excited fluorescence spectrum for the inhomogeneously broadened ensemble of systems is obtained by convolution of the single site/state spectrum with their distribution function (SDF) $N(\Omega - \omega_\mathrm{C})$ peaking at $\omega_\mathrm{C}$. It is usually taken that the SDF has a Gaussian shape.

The FLN spectrum, $F(\omega)$, selectively excited at $\omega_\mathrm{E}$ is given as

$$F(\omega) = \sum_{R,P=0}^{\infty} \left(S^R \frac{\mathrm{e}^{-S}}{R!}\right)\left(S^P \frac{\mathrm{e}^{-S}}{P!}\right) \int \mathrm{d}\Omega\, N(\Omega - \omega_\mathrm{C}) l_R(\omega - \Omega + R\omega_\mathrm{m}) l_P(\omega_\mathrm{E} - \Omega - P\omega_\mathrm{m}) \quad (2)$$

## 3. Experimental Results

Generally, two different types of line-narrowing experiments were performed with all samples by recording (i) HB and (ii) FLN spectra at 5 K. The former series also included ZPH action and hole depth saturation studies, while the latter one, the ΔFLN measurements. Before presenting the line-narrowing results, for an overview, we first describe the conventional (broadband) absorption and fluorescence spectra of the complexes measured at low temperatures (Figure 1). The $Q_y$ absorption spectrum of LH2 (Figure 1a) exhibits bands near 800 and 850 nm (with full width at half maximum (fwhm) of 125 and 270 $\mathrm{cm}^{-1}$, respectively) corresponding to the arrangement of the BChl molecules into two rings, often referred as the B800 and B850 rings.[2] The fluorescence (dashed line) was excited at 800 nm. The fluorescence spectrum with a peak at 872.2 nm (11465 ± 5 $\mathrm{cm}^{-1}$) is strongly asymmetric, like its absorption counterpart, but it is considerably broader (fwhm of 292 ± 10 $\mathrm{cm}^{-1}$). The absorption spectrum of the LH1 complex (Figure 1b) contains a lone B875 band at 886.1 nm corresponding to the cyclic 15- or 16-mer of BChl dimers. Its fluorescence, excited into the blue edge of the absorption band at 845 nm, has a maximum at 901.5 nm (11093 ± 5 $\mathrm{cm}^{-1}$). As for LH2, the shape of the fluorescence band is more extended towards longer wavelengths, but it is narrower (fwhm of 233 ± 10 $\mathrm{cm}^{-1}$) than the corresponding absorption band (~259 $\mathrm{cm}^{-1}$). It is also noteworthy that there is a considerably larger Stokes shift between the related absorption and fluorescence spectra in LH2 (~301 $\mathrm{cm}^{-1}$) when compared to that in LH1 (~192 $\mathrm{cm}^{-1}$).

**Hole-Burning Data.** Figure 1 also shows the ZPH action spectra, that is, the distribution of ZPH depths for both complexes. The ZPH action spectroscopy is used to find spectral position and shape of the SDF of absorbing substances subject to hole burning. Under the conditions of the present experiment, the fractional depths of ZPH (defined as the absorbance change divided by the initial absorbance) were less than 0.08 so that saturation effects would not significantly affect the shape of the action spectrum. In agreement with our earlier studies, the action spectrum of LH2 complexes can be fitted with a Gaussian peaking at 11 562 ± 5 $\mathrm{cm}^{-1}$ (864.9 nm) and having a fwhm of 147 ± 10 $\mathrm{cm}^{-1}$.

In the LH1 complex the ZPH action spectrum is narrower (fwhm of 119 ± 10 $\mathrm{cm}^{-1}$) than for LH2. It peaks at 11 161 ± 5 $\mathrm{cm}^{-1}$ (896.0 nm). This is the so-called B896 sub-band of the B875 absorption band.[4] We notice a smaller energy gap between the B875 and B896 bands (124 ± 5 $\mathrm{cm}^{-1}$) in LH1 compared with the gap between the B850 and B870 bands (204 ± 5 $\mathrm{cm}^{-1}$) in LH2, in fulfillment of expectations based on higher density of exciton states in LH1 complexes.

For the LH1 membranes (not shown), the shape of the absorption spectrum is similar to the one for LH1 complexes, but shifted further to the red by ~27 $\mathrm{cm}^{-1}$. Also similar is the B896 bandwidth (~121 $\mathrm{cm}^{-1}$), which affirms the high quality of isolated complexes we study: the necessarily harsh isolation treatment has not visibly broadened the SDF of the isolated complexes. Yet, the gap between the ZPH action spectrum and the absorption maximum in LH1 membranes (~144 $\mathrm{cm}^{-1}$) is larger by ~20 $\mathrm{cm}^{-1}$ than in LH1 complexes. This is in agreement with previous measurements[6] where a gap of 140 $\mathrm{cm}^{-1}$ has been reported, although for the B896 band of somewhat larger width (150 ± 10 $\mathrm{cm}^{-1}$). In all samples studied poor mirror symmetry of related absorption and emission spectra relative to the ZPL action spectrum is observed.

Figure 2 shows the fluence-dependent HB spectra in LH1 and LH2 complexes at burn wavelengths of $\lambda_\mathrm{B}$ = 898.1 and 867.0 nm, respectively, with burn fluences ranging from 0.02 to 94 J/$\mathrm{cm}^2$. Fractional optical density changes at $\lambda_\mathrm{B}$ are indicated. The sharp hole coincident with the burn wavelength is the ZPH. The width of the ZPH is limited by the read resolution of 1.2 $\mathrm{cm}^{-1}$. At higher burn fluences it is also affected by the saturation broadening. The features just to the left and right of the ZPH are the real- and pseudo-PSB holes, respectively. On both sides of the burn wavelength are relatively narrow regions of increased absorbance called an antihole. The origin of the antihole is an induced absorbance due to photoproducts of hole burning. The antihole becomes more visible at higher burn fluences due to saturation of ZPH, and it strongly interferes with both real- and pseudo-PSB holes. The distribution function of HB photoproducts and their absorption spectra are generally not known, moreover the limited width of the SDF obstructs the direct assessment of the PSB from the HB spectrum. The photoproducts should, at least in principle, also concern the ΔFLN spectra. In practice, however, and this will be demonstrated below, the ΔFLN measurements are superior to the HB ones in providing far more reliable information about the PSB.

As can be seen from Figure 2, the burning efficiency at low fluences is 2−3 times higher in LH1 than it is in LH2.

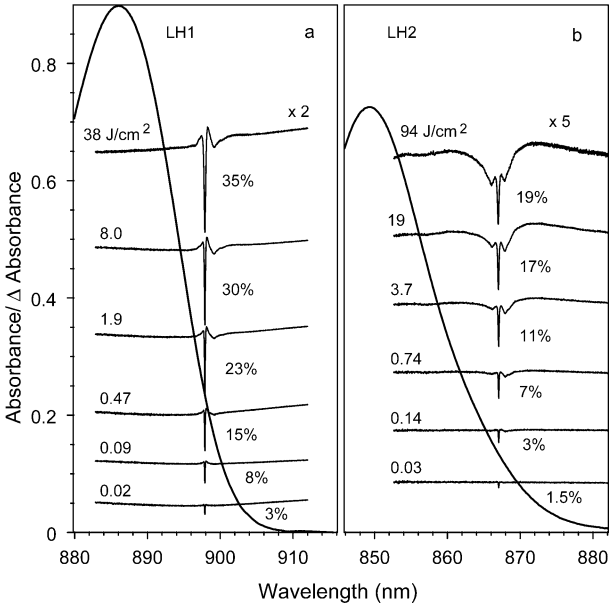


**Figure 2.** Absorption and hole spectra of LH1 (a) and LH2 (b) complexes from *Rb. sphaeroides* at 5 K. The hole spectra for LH1 obtained with $\lambda_B = 898.1$ nm are magnified 2 times relative to the absorbance scale and shifted vertically with respect to each other for better observation. The hole spectra for LH2 are obtained at $\lambda_B = 867.0$ nm and magnified 5 times.

Furthermore, the fractional saturated hole at similar energetic distance from the B870/B896 band maximum toward longer wavelengths is over two times deeper in LH1 than in LH2, if normalized to the same fluence. This suggests that the electron−phonon coupling in LH1 should be weaker than in LH2.

**Double Selective Fluorescence Data.** Figure 3a shows the FLN spectra of LH2 complexes excited at $\lambda_E = 869$ nm taken before (top curve) and successively after hole-burning exposures of 1.5, 6.4, and 170 J/cm$^2$. The laser wavelength was kept unchanged during consecutive steps of hole burning and fluorescence measurements, that is, $\lambda_E = \lambda_B =$ constant. We notice an unusually weak excitation laser scattering peak overlapping with the ZPL and a very good signal-to-noise ratio achieved in these measurements. Although excited selectively, the observed fluorescence (side)band remains broad and almost featureless, in agreement with previous selective fluorescence spectroscopy data.[7,10,20] The fwhm of the band at 0.04 J/cm$^{-2}$ is ∼270 cm$^{-1}$, and its peak is red-shifted relative to the excitation by ∼115 cm$^{-1}$.

Figure 3b shows the fluence dependence of the integral intensity of the FLN spectra for LH1 and LH2 complexes at burn wavelengths of $\lambda_B = 902$ and 869 nm, respectively. The dependence for both complexes is similar over experimental burn fluences covering nearly 4 orders of magnitude, from 0.04 to 200 J/cm$^2$. An important finding is that the burn fluence range can clearly be separated into two parts characterized with fairly different hole-burning efficiency: the high-efficiency region at low-burning fluences and the low-efficiency one at high fluences. The partition point is at around 1.0 J/cm$^2$, a remarkably low fluence. The FLN data also confirm the conclusions made from HB measurements that burning efficiency in LH1 is larger than in LH2 and so is the saturated hole depth.

Figure 4a shows the initial and high-fluence postburn (at burn fluence of 170 J/cm$^2$) FLN spectra for LH2 complexes at 869 nm excitation. Also shown is a ΔFLN spectrum obtained at small (1.5 J/cm$^2$) fluence. As seen, the ΔFLN spectrum is blue-shifted, narrower, and also much more structured than either of the FLN spectra. It has a well-resolved ZPL and an asymmetric

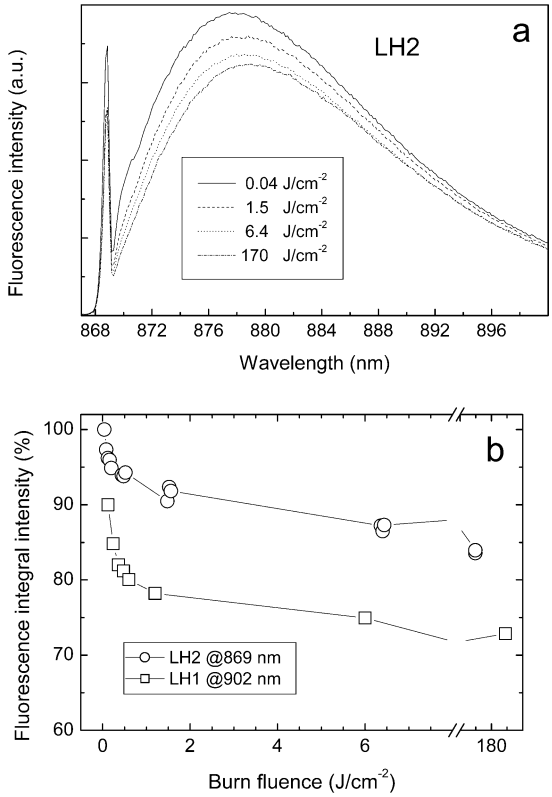


**Figure 3.** (a) Fluorescence line-narrowing spectra of LH2 complexes from *Rb. sphaeroides* at 5 K at different light exposures. (b) Relative integrated intensity of LH1 and LH2 FLN spectra as a function of burn fluence.

PSB where a low-frequency peak at ∼20 cm$^{-1}$ and a secondary broad maximum at ∼50−60 cm$^{-1}$ can be distinguished. The PSB spectrum in Figure 4a is almost identical to the one reported before.[8] One can also conclude that the scattering contribution into the origin of the FLN spectra is indeed very small and measures with the intensity of the ZPL. Saturation at larger exposures (not shown) reveals a small broadening of the PSB and also a loss of ZPL intensity (indicating that the apparent Huang−Rhys factor increases with fluence, see Figure 5 below).

The double selection fluorescence spectroscopy was applied to purified LH1 antenna complexes for the first time. Figure 4b shows the result for a narrow-band excitation at $\lambda_E = \lambda_B =$ 902 nm. Although the initial FLN spectrum is relatively broad (fwhm is ∼218 cm$^{-1}$), it reveals some structure, which is much more strongly expressed than that in LH2. The initial spectrum has a flat peak red-shifted relative to the excitation by ∼60 to 100 cm$^{-1}$. High-fluence exposure of the sample to laser light resulted in a significant (∼30%) decrease of the fluorescence yield and in a complete wipeout of the structure. The difference fluorescence signal has a ZPL, stronger than in LH2, and an asymmetric PSB with two rather well-resolved frequencies at ∼30 and ∼100 cm$^{-1}$. Apart from the fine details, rather similar band shapes of ΔFLN and postburn FLN spectra are apparent, in contrast to the situation for the LH2 complex. The difference fluorescence signal increases under additional hole-burning exposures but its shape remains. A general similarity of the PSB shapes of the differential FLN spectra of the LH1 and LH2 complexes is also worth noticing here, although this is not so evident without direct overlapping of the area-normalized spectra.

Figure 5 shows an apparent Huang−Rhys factor estimated from the experimental ΔFLN spectra as a function of burn fluence. The following equation was used to calculate the

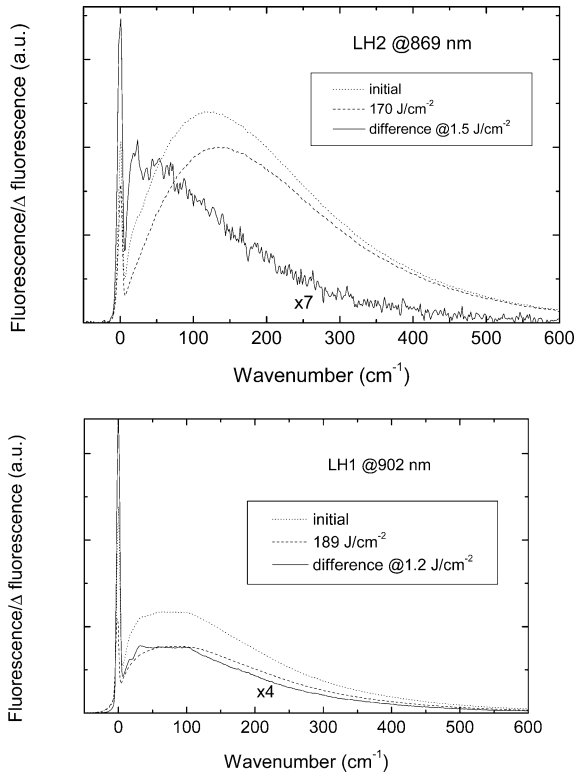


**Figure 4.** Fluorescence line-narrowing and differential FLN spectra of LH2 (a) and LH1 (b) complexes from *Rb. sphaeroides* at 5 K. Shown in both frames are initial (no burn) and high-burn (burn fluence of 189 J/cm$^2$ for LH1 and of 170 J/cm$^2$ for LH2) FLN spectra together with low-burn differential FLN spectra. The latter were obtained by subtracting the low-burn FLN spectra (burn fluence of 1.2 J/cm$^2$ for LH1 and of 1.5 J/cm$^2$ for LH2) from the initial spectra. The differential spectra are magnified 4 (LH1) or 7 (LH2) times for better visibility.

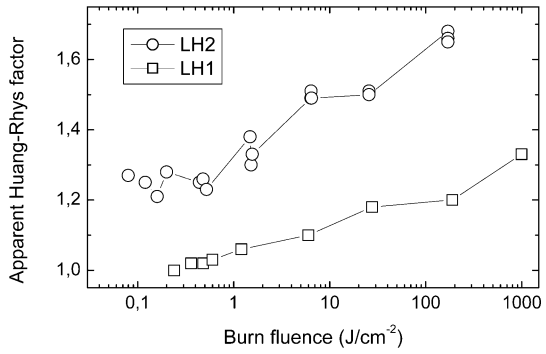


**Figure 5.** Apparent Huang−Rhys factor determined from differential FLN spectra of LH1 and LH2 complexes as a function of burn fluence. Notice the logarithmic *x*-scale.

Huang−Rhys factor, $S$: $e^{-2S} = \int \mathrm{ZPL}(\omega)\, d\omega / \int \Delta\mathrm{FLN}(\omega)\, d\omega$, where integrations over the whole differential fluorescence spectrum and ZPL were considered on the frequency scale. As seen, the apparent Huang−Rhys factor is greater than one in both complexes, suggesting a rather strong electron−phonon coupling. The coupling generally increases with fluence.

The precise amount of scattered laser light in the differential FLN spectra is unknown. This can lead to a systematic error by *decreasing* the apparent Huang−Rhys factor. Although it is difficult to quantify this potential mistake, we believe that it is most probably insignificant judging from the constancy of the apparent Huang−Rhys factor at low-burn fluence range. There, however, is another factor that prevents the Huang−Rhys factor being directly derived from the selective-spectroscopy data. The PSB in the ΔFLN spectra consists of several spectral components, from which only one is the real PSB (see Materials and Methods). Ignoring this circumstance leads to an *increase* of the apparent Huang−Rhys factor relative to the actual one. In the following section we apply a model of Hayes et al.[17] and Pieper et al.[18] for assessment of correct spectral shapes and *S* factors based on low-fluence experimental differential FLN spectra.

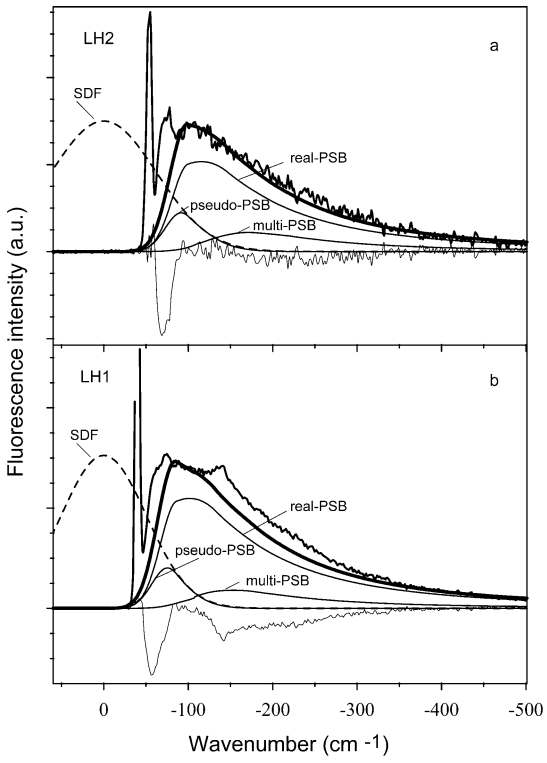


**Figure 6.** Fit of sidebands of experimental differential FLN spectra (noisy curves) for LH2 (a) and LH1 (b) complexes. The calculated spectrum (bold continuous curve) was obtained using parameters given in Table 1. The three multiphonon contributions to the calculated spectrum are labeled as real-PSB, pseudo-PSB and multi-PSB; see text for explanations. The state distribution function (dashed line) is shown for reference.

## 4. Discussion

**Simulations of Differential FLN Spectra.** A characterization of electron−phonon coupling within the framework of the model of refs 17 and 18 requires the knowledge of the peak position $\omega_C$ and shape/width of the SDF, the Huang−Rhys factor, as well as of the spectral shapes of the ZPL and one-phonon PSB profile $l_1(\omega - \Omega \mp \omega_m)$. The parameters of the SDF can reliably be determined from the HB experiment. We further concentrate on the one-phonon profile. Apart from small details, the ΔFLN spectra suggest that the one-phonon profile should generally be of asymmetric shape peaking at ∼50 to 60 cm$^{-1}$ in both the LH1 and LH2 complexes. This information allows an initial guess of the one-phonon profile, which for computational ease was constructed from a sum of Gaussian (low-frequency side) and Lorentzian (high-frequency side) parts, similar for both complexes. Modifying the one-phonon profile parameters and the *S* factor iteratively, we then aimed at the best fit of measured and calculated ΔFLN spectra.

Figure 6 illustrates part of the simulation procedure. The positive-amplitude noisy curves in Figure 6 represent the experimental ΔFLN spectra and the smooth continuous curves, the calculated spectra. From eq 2, three types of contributions to the calculated PSB can be identified. The $P = 0$, $R \geq 1$ terms

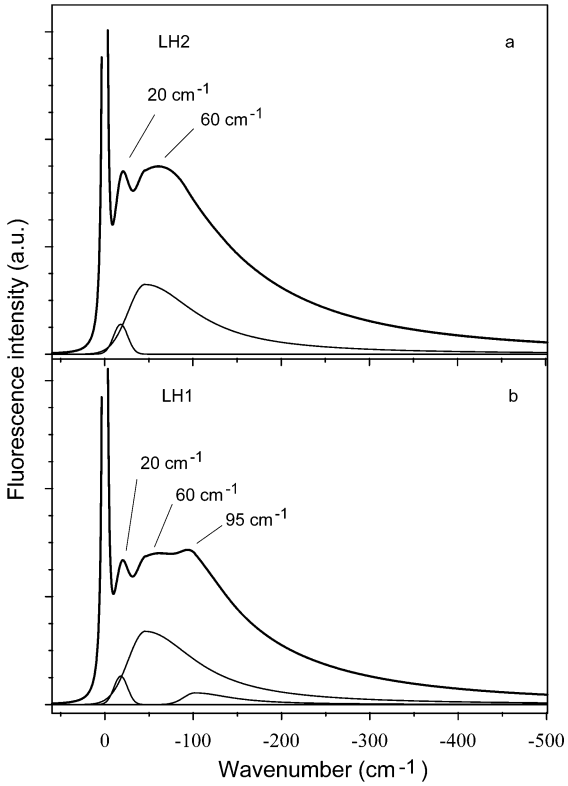


**Figure 7.** The calculated homogeneous fluorescence spectra related to the B870 (a) and B896 (b) absorption bands. The ZPL is cut off at 3% of its peak intensity value. The corresponding one-phonon profiles (not in scale) are shown at the bottom of the figure.

represent phonon transitions that are excited resonantly via the ZPL. They form the real-PSB. The $P \geq 1$, $R = 0$ terms correspond to electronic transitions which are nonresonantly excited via their PSB. The zero-phonon lines of these transitions constitute the pseudo-PSB. Finally, the $R$, $P \neq 0$ multiphonon terms represent the PSB of the ZPL associated with the pseudo-PSB (the multi-PSB).

As seen from Figure 6, the main part of the experimental PSB is well reproduced using a single asymmetric Gaussian/Lorentzian one-phonon profile with a maximum at 50 $cm^{-1}$. The Gaussian side half-width is 46 $cm^{-1}$, while that of the Lorentzian side is 140 $cm^{-1}$. The PSB has a main contribution from the real-PSB. However, the pseudo-PSB and multi-PSB components cannot also be neglected. In the case of the red wing excitation, the high-frequency tail of the pseudo-PSB signal is effectively suppressed by the limited width of the SDF, which is clear from inspection of the figure. In addition, small but significant parts of the sideband could not be fitted by the sole one-phonon profile applied. They are shown as negative-amplitude noisy curves in Figure 6 obtained as a difference between the calculated and measured PSB. To account for these differences one (LH2) or two (LH1) more frequency components were added. Positions of the additional components needed are evident from the negative-amplitude spectra on Figure 6.

Figure 7 concludes this part of the study by presenting the homogeneous fluorescence spectra and one-phonon profiles related to the B870 and B896 states. The homogeneous spectra are calculated according to eq 1 using the same parameters as deduced from fittings of the ΔFLN spectra. The ZPL at the origin, assumed to have a 1.2 $cm^{-1}$ fwhm (which is the experimental resolution), is cut off at ~3% of its peak intensity value. As seen for both samples, the shape of the PSB is strongly asymmetric toward longer wavelengths as well as being

**TABLE 1: Linear Electron−Phonon Coupling Parameters for the B870 and B896 States in LH1 and LH2 Antenna Complexes of *Rb. sphaeroides*[a]**

| | Δ | $S_1$ | $\omega_1$ | $\Gamma_{G1}$ | $S_2$ | $\omega_2$ | $\Gamma_{G2}/2$ | $\Gamma_{L2}/2$ | $S_3$ | $\omega_3$ | $\Gamma_{G3}/2$ | $\Gamma_{L3}/2$ |
|---|---|---|---|---|---|---|---|---|---|---|---|---|
| LH1 | 119 | 0.04 | 18 | 18 | 0.75 | 46 | 46 | 140 | 0.07 | 102 | 30 | 100 |
| LH2 | 147 | 0.06 | 18 | 18 | 1.0 | 46 | 46 | 140 | | | | |

[a] $S_1$, $S_2$, and $S_3$ are the Huang−Rhys factors for the phonon distributions with peak frequencies of $\omega_1$, $\omega_2$, and $\omega_3$; $\Gamma_{G1}$, $\Gamma_{G2}$, $\Gamma_{L2}$, $\Gamma_{G3}$ and $\Gamma_{L3}$ are the fwhm of these (Gaussian or Lorentzian) distributions (see text for details). Δ is the fwhm of the site distribution function. All units are in wavenumbers, except dimensionless Huang−Rhys factors.

structured. In LH2 the most prominent structural elements are two peaks at 20 and 60 $cm^{-1}$ related to phonon frequencies of $\omega_1 = 18$ $cm^{-1}$ and $\omega_2 = 46$ $cm^{-1}$. Only the 18-wavenumber peak was identified by HB spectroscopy.[4,6] The total $S$ factor is 1.05 ± 0.10, slightly larger than the previously reported number[8] reflecting the fitting uncertainties. Seen in LH1 are the same two peaks and an additional broad shoulder at 95 $cm^{-1}$ related to a frequency of $\omega_3 = 102$ $cm^{-1}$. The total $S$ factor in LH1 is 0.85 ± 0.10, considerably less than in LH2. The two lower phonon frequencies (around 19 and 50 $cm^{-1}$) were also observed in FLN spectra of the B820 complex,[21] a subunit of LH1. The PSB components used are shown as one-phonon profiles at the bottom of parts a and b of Figure 7. The fit parameters and distribution of electron−phonon coupling strength among different phonon components are given in Table 1.

The origin of the PSB structure is left for future studies. Here we only notice that the shape of the main sideband component with a maximum at ~50 $cm^{-1}$ is similar to the density of phonon states in prototype proteins.[22] Then the other structures reflect the local dynamics characteristic to antenna complexes.

**Heterogeneous Nature of Antenna Fluorescence.** The observations shown in Figure 4a strongly suggest that the fluorescence band in the LH2 antenna complexes consists of two contributions, of which hole burning effectively modifies only the blue-sided and more structured component. In absorption this component is connected to the B870 band. The remaining contribution to the FLN spectrum is broadband and structureless. This component has to originate from other types of electronic states that absorb in the same 870 nm region but are less sensitive to hole burning. After burning with the exposures larger than 1 $J/cm^2$ the B870 states are burnt out almost to the saturation ZPH depth (see Figures 3b and 4a). Therefore, the remaining after hole burning FLN spectrum in Figure 4a should largely represent the second fluorescence component. Its maximum is red-shifted relative to the excitation by ~138 $cm^{-1}$, essentially more than it was in the nonirradiated spectrum (~115 $cm^{-1}$). Such a broad and structureless fluorescence spectrum is characteristic of systems with strong electron−phonon coupling, and primarily for this reason it was assigned to self-trapped excitons.[7]

From another approach, the broadband fluorescence spectra can be simulated using selective-spectroscopy data (Figure 8). The blue sub-band in Figure 8a is obtained by convoluting the single-complex spectrum of Figure 7 with a 147 $cm^{-1}$ broad Gaussian SDF and by adjusting its intensity according to the blue side of the LH2 fluorescence spectrum. Subtracting the blue sub-band from the overall spectrum then results in the red sub-band, which looks fairly similar to the FLN spectrum in Figure 4a left after saturating hole-burning exposure. Taking the one-phonon profile related to the B870 states (Figure 7) as

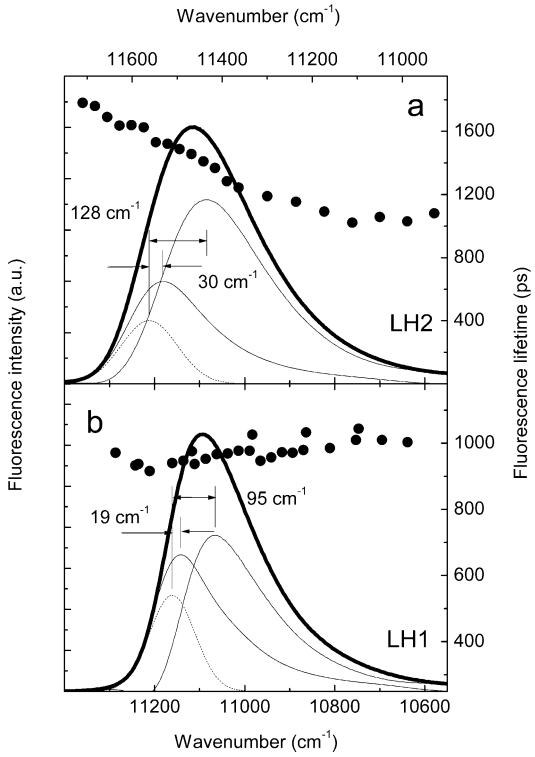


**Figure 8.** A result of a spectral decomposition of nonselectively excited fluorescence spectra (bold solid curves) based on selective-spectroscopy data (see text for explanations) and spectral dependence of fluorescence lifetime (dots) for LH2 (a) and LH1 (b) complexes at 5 K. Dashed curves represent the SDF.

a reference, one can estimate that the effective *S* factor for the red sub-band is between 2.5 and 2.8.

Further support for a heterogeneous composition of the LH2 antenna emission comes from the fluorescence decay time dependence on recording wavelength. As seen from Figure 8a, the fluorescence lifetime, being equal to ~1.8 ns on the blue side of the spectrum, does not stay constant but gradually decreases to ~1.1 ns at its red side. Analysis shows[5,9] that the observed fluorescence lifetime dependence can be explained with spectral heterogeneity very similar to the one in Figure 8a. All these arguments combined together seem to validate quite clearly that in LH2 there is always an additional emission component present that is broader and considerably further red-shifted as compared to the B870 fluorescence, both under resonant and nonresonant excitation.

For LH1 the presence of two fluorescence contributions is less obvious, as differences between the FLN and ΔFLN signals are much smaller (see Figure 4b). The virtual absence of the dependence of the fluorescence decay time on recording wavelength in Figure 8b lends no support to this hypothesis either, although it does not exclude it. However, from the mere fact that there is a difference between the postburn FLN and ΔFLN signals it follows that some spectral heterogeneity must exist. The decomposition shown in Figure 8b, analogous to the analysis for LH2, suggests a considerable amount of the red component. The effective *S* factor for this band can be estimated as between 1.9 and 2.1. Considering the roughness of the applied approach, these numbers await further refinement.

The absence of the fluorescence decay time dependence on recording wavelength in Figure 8b is of special interest. In LH1-containing membranes a characteristic fluorescence spectral red shift has long been observed in the picosecond time scale at low temperatures.[23−26] This was ascribed to energy transfer between spectrally heterogeneous antenna complexes within large photosynthetic membranes. A confirmation of this assumption was first obtained when excitation kinetics in isolated and native membrane-embedded LH2 complexes was comparatively studied.[13] The progress with LH1 antennas has been slow due to difficulties in finding proper isolation procedures of the complex. The data of Figure 8b can thus be considered as a first clarification of the long-standing problem concerning the core antenna. The picosecond decay components observed in membranes[23−26] and absent in isolated complexes (Figure 8b) are due to energy transfer between LH1 complexes.

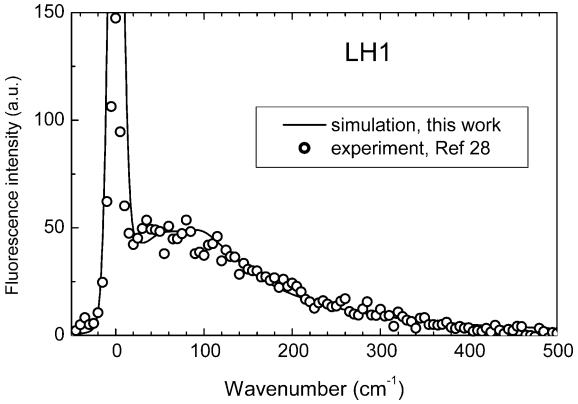


**Figure 9.** Comparison of low-temperature experimental (dots, data from ref 28) and calculated (continuous curve, the same as in Figure 7a) fluorescence spectra for LH1 complexes.

**Comparison With Single-Molecule Fluorescence Data.** It is of interest to compare the present selective-spectroscopy results on antenna ensembles with the low-temperature fluorescence spectra of single LH1 and LH2 complexes. Measurements of single LH2 antennas from *Rhodopseudomonas acidophila* show relatively broad fluorescence spectra of greatly varying shapes for different complexes.[27] A closer inspection of all available spectra, however, clearly reveals two predominant contributions into the spectra, the narrower blue and broader, but stronger, red ones. The spectra have been taken at relatively high temperatures (9.5 K being the lowest temperature reported), which along with spectral diffusion probably explains why the narrow ZPL was not recorded.

Also the LH1 single-complex spectra demonstrate a great variety of line shapes, however, differently from LH2, an image of a narrow ZPL is almost always present.[28] This probably can be explained with lower experimental temperature (1.8 K) along with weaker electron−phonon coupling in LH1 as compared with LH2. Figure 9 compares one of the finest-looking single-molecule spectra from ref 28 with the homogeneous spectrum obtained from the present work. To meet the experimental resolution, the homogeneous spectrum from Figure 7a was convoluted with a 16.5 $cm^{-1}$ fwhm Gaussian. As seen, the fit of the PSB is almost perfect, while the calculated ZPL peak is about two times higher compared to the experimental one. Considering the different sources of the LH1 complexes studied (from *Rb. sphaeroides* in this work and from *Rhodospirillum rubrum* in ref 28), the match is beyond expectations.

## 5. Summary

The fluorescence of core LH1 and peripheral LH2 antenna complexes from the photosynthetic bacterium *Rb. sphaeroides* has been studied at 5 K upon selective excitation at the red tail of the exciton absorption band. It was shown using the double spectral selection technique that the fluorescence in both complexes consists of two overlapping contributions. On the

basis of earlier work,[7,10] we assign these contributions to the relatively weakly coupled nearly free excitons and to the more strongly coupled dynamically self-trapped excitons. The apparent phonon structure of nearly free excitons has been analyzed resulting in a single-exciton state absorption/emission profile. The main part of the profile in both complexes consists of a broad asymmetric PSB with a maximum at 50 $cm^{-1}$. The density of phonon states in proteins typically has such a shape.[22] The total Huang−Rhys factor is equal to $S = 0.85 \pm 0.10$ in LH1 and $S = 1.05 \pm 0.10$ in LH2. Both numbers are larger than usually considered. We notice that the moving exciton feels a phonon field much less than does the localized excitation. The Huang−Rhys factor calculated for localized Bchl excitations in the protein surroundings is thus expected to be considerably larger than one, the number recently proposed in ref 29 for the B777 monomer pigment−protein complex of LH1. For reference, the intensity of the PSB relative to that of the ZPL in exciton spectra is reduced by a factor of $(\varpi/2dV)^{d/2}$, where $\varpi$ is the mean vibrational frequency, $V$ is the exciton coupling energy, and $d$ is the dimensionality of the lattice.[30] This qualitatively corroborates our conclusions concerning the remaining (red-shifted) fluorescence component, which was assigned to the more localized excitons. Excitonic polarons are thus proper excitations in LH1 and LH2, as the electron−phonon coupling cannot be ignored.

**Acknowledgment.** The Estonian Science Foundation (Grant No. 5543), Hasselblad Foundation, and the EstoMaterials program of the EC "Center of Excellence" have supported this work. The authors are grateful to C. Tietz for sharing the single-molecule data used in Figure 9 and to N. W. Woodbury for kindly providing the LH2 samples.

## References and Notes

(1) van Amerongen, H.; Valkunas, L.; van Grondelle, R. *Photosynthetic Excitons*; World Scientific: Singapore, 2000.

(2) Papiz, M. Z.; Prince, S. M.; Howard, T.; Cogdell, R. J.; Isaacs, N. W. *J. Mol. Biol.* **2003**, *326*, 1523−1538.

(3) Roszak, A. W.; Howard, T. D.; Southall, J.; Gardiner, A. T.; Law, C. J.; Isaacs, N. W.; Cogdell, R. J. *Science* **2003**, *302*, 1969−1972.

(4) Reddy, N. R. S.; Picorel, R.; Small, G. J. *J. Phys. Chem.* **1992**, *96*, 6458−6464.

(5) Freiberg, A.; Rätsep, M.; Timpmann, K.; Trinkunas, G.; Woodbury, N. W. *J. Phys. Chem. B* **2003**, *107*, 11510−11519.

(6) Wu, H.-M.; Rätsep, M.; Jankowiak, R.; Cogdell, R. J.; Small, G. J. *J. Phys. Chem. B* **1998**, *102*, 4023−4034.

(7) Freiberg, A.; Rätsep, M.; Timpmann, K.; Trinkunas, G. *J. Lumin.* **2003**, *102*−*103*, 363−368.

(8) Rätsep, M.; Freiberg, A. *Chem. Phys. Lett.* **2003**, *377*, 371−376.

(9) Freiberg, A.; Rätsep, M.; Timpmann, K.; Trinkunas, G. *J. Lumin.*, in press.

(10) Timpmann, K.; Katiliene, Z.; Woodbury, N. W.; Freiberg, A. *J. Phys. Chem. B* **2001**, *105*, 12223−12225.

(11) Jones, M. R.; Fowler, G. J. S.; Gibson, L. C. D.; Grief, G. G.; Olsen, J. D.; Crielaard, W.; Hunter, C. N. *Mol. Microbiol.* **1992**, *6*, 1173−84.

(12) Walz, T.; Jamieson, S. J.; Bowers, C. M.; Bullough, P. A.; Hunter, C. N. *J. Mol. Biol.* **1998**, *282*, 833−845.

(13) Timpmann, K.; Woodbury, N. W.; Freiberg, A. *J. Phys. Chem. B* **2000**, *104*, 9769−9771.

(14) Fünfschilling, J.; Glatz, D.; Zschokke-Gränacher, I. *J. Lumin.* **1986**, *36*, 85−92.

(15) Bogner, U.; Schwarz, R. *Phys. Rev. B* **1981**, *24*, 2846−2849.

(16) Freiberg, A.; Saari, P. *IEEE J. Quantum Electron.* **1983**, *QE*−*19*, 622−30.

(17) Hayes, J. M.; Gillie, J. K.; Tang, D.; Small, G. *J. Biochim. Biophys. Acta* **1988**, *932*, 287−305.

(18) Pieper, J.; Voigt, J.; Renger, G.; Small, G. J. *Chem. Phys. Lett.* **1999**, *310*, 296−302.

(19) Pieper, J.; Schödel, R.; Irrgang, K.-D.; Voigt, J.; Renger, G. *J. Phys. Chem. B* **2001**, *105*, 7115−7124.

(20) Visschers, R. W.; Germeroth, L.; Michel, H.; Monshouwer, R.; van Grondelle, R. *Biochim. Biophys. Acta* **1995**, *1230*, 147−154.

(21) Creemers, T. M. H.; De Caro, C. A.; Visschers, R. W.; van Grondelle, R.; Volker, S. *J. Phys. Chem. B* **1999**, *103*, 9770−9776.

(22) Elber, R.; Karplus, M. *Phys. Rev. Lett.* **1986**, *56*, 394−397.

(23) Freiberg, A.; Godik, V. I.; Timpmann, K. In *Progress in Photosynthesis Research*; Biggins, J., Ed.; Nijhoff: Dordrecht, The Netherlands, 1987; pp 45−8.

(24) Freiberg, A.; Timpmann, K. *J. Photochem. Photobiol.* **1992**, *B15*, 151−8.

(25) Timpmann, K.; Freiberg, A.; Godik, V. I. *Chem. Phys. Lett.* **1991**, *182*, 617−22.

(26) Hunter, C. N.; Bergström, H.; van Grondelle, R.; Sundström, V. *Biochemistry* **1990**, *29*, 3203−3207.

(27) Tietz, C.; Chekhlov, O.; Dräbenstedt, A.; Schuster, J.; Wrachtrup, J. *J. Phys. Chem. B* **1999**, *103*, 6328−6333.

(28) Gerken, U.; Jelezko, F.; Götze, B.; Branschädel, M.; Tietz, C.; Ghosh, R.; Wrachtrup, J. *J. Phys. Chem. B* **2003**, *107*, 338−343.

(29) Renger, T.; Marcus, R. A. *J. Chem. Phys.* **2002**, *116*, 9997−10019.

(30) Ueta, M.; Kanzaki, H.; Kobayashi, K.; Toyozawa, Y.; Hanamura, E. *Excitonic Processes in Solids*; Springer: Berlin, 1986.